Contribution from the Department of Chemistry and Biochemistry, The University of Texas at Austin, Austin, Texas 78712

Effects of Substituents on the Spectral and Redox Properties of Cadmium(II) Texaphyrins

Bhaskar G. Maiya, Thomas E. Mallouk,* Gregory Hemmi, and Jonathan L. Sessler*

Received May 22, 1990

The synthesis, electronic absorption spectra, and electrochemistry of cadmium(II) texaphyrins substituted with various electron-donating or electron-withdrawing groups are described. The one-electron oxidation and reduction potentials and the energies of the lowest energy absorption band maxima (λ_Q 754–797 nm) are sensitive to the nature of substituents attached to the phenyl ring of these novel pentadentate macrocycles. Cyclic voltammetric data revealed that weakly binding counterions associated with these monopositive complexes (e.g. ClO_4^- or NO_3^-) dissociate upon one-electron reduction; the reduction peaks are irreversible to quasi-reversible in these cases. However, in the presence of strongly binding chloride ion (Cl^-) or nitrogen bases (e.g. pyridine), the reduction process is electrochemically revesible and ligand dissociation does not occur on the cyclic voltammetric time scale. A linear relationship between the frequency of the lowest energy absorption maximum and the difference in potentials for the first oxidation and reduction processes (1.54–1.40 V) exists in these systems. A similar relationship was also found for those texaphyrin complexes in which the phenyl group is replaced by a naphthyl, phenanthryl, or dicyano group. These results are discussed on the basis of the known spectral and redox features of metalloporphyrins.

Introduction

Our efforts to develop aromatic (22-π-electron), pentadentate, porphyrin-like macrocyclic complexes[1] have resulted in the discovery of a tripyrrole–dimethyl-derived cadmium(II) "expanded porphyrin" complex ("texaphyrin", $[(TXP)Cd]^+$).[2] This complex and the corresponding zinc(II) analogue show a strong, low-energy visible absorption band centered at 760 nm, have high triplet quantum yields, and act as efficient photosensitizers for the production of singlet oxygen ($^1O_2$) in methanol solution.[3] Detailed investigations have been carried out on the structure and electron-transfer reactions of the $[(TXP)Cd]^+$ triplet state by using time-resolved ESR[4] and laser flash-photolysis[5] techniques. The ground- and excited-state properties of these complexes, and their good chemical stability, suggest that texaphyrins could serve as viable photosensitizers in photodynamic therapy (PDT) and related biomedical applications where a photoactive dye possessing an intense absorption in the physiologically transparent region (i.e 700 nm $< \lambda <$ 900 nm) is needed.[6] Indeed, in preliminary in vitro studies with $[(TXP)Cd]^+$ in 10% human serum a significant decrease in herpes simplex (HSV-1) infectivity and lymphocyte mitogenic activity have been observed upon irradiation at 767 nm.[7]

A comprehensive understanding of the physicochemical properties of the texaphyrins is crucial in evaluating these complexes for PDT and related applications. Specifically, it is important to identify the factors that influence the absorption and redox features of texaphyrin photosensitizers, since these factors are vital determinants to their in vivo photodynamic activity as photosensitizers in PDT. This study is aimed at a realization of this theme, and here we extend the expanded porphyrin concept to several new members of the texaphyrin family of complexes having varied structures (and, consequently, properties). We report here the synthesis and the spectral and electrochemical characteristics of new cadmium(II) texaphyrins with electron-withdrawing or -donating substituents directly attached to the phenyl group of the macrocycle (Figure 1). In addition, we report the spectral and electrochemical properties of texaphyrins in which either a naphthyl ($[(NPTXP)Cd]^+$), a phenanthryl ($[(PNTXP)Cd]^+$), or a dicyano ($[(CNTXP)Cd]^+$) (Figure 2) group is attached to the main frame of the macrocycle.

Experimental Section

(a) Materials. All solvents and reagents were of AR or Spectrograde quality and were used as received unless otherwise noted. Tetra-*n*-butylammonium perchlorate ($(TBA)ClO_4$) was purchased from Kodak Laboratory Chemicals and was recrystallized twice from anhydrous ethanol and stored under vacuum before use. Tetra-*n*-butylammonium chloride ((TBA)Cl), obtained from Aldrich, was used as received. The CH_2Cl_2 used for cyclic voltammetric measurements was distilled from CaH_2.

The substituted *o*-phenylenediamine-derived texaphyrins (Figure 1) were synthesized by using the general method[2] developed for the synthesis of the original texaphyrin $[(TXP)Cd]^+$ as outlined briefly as follows: 2,5-Bis((3-ethyl-5-formyl-4-methylpyrrol-2-yl)methyl)-3,4-diethylpyrrole[1b] (1 mmol) and the corresponding substituted diaminobenzene (each 0.9 mmol) were heated at reflux overnight in a mixture of benzene and methanol (1.0:0.2 v/v, 500 mL), after which the solvents were evaporated. The residue was recrystallized in CH_2Cl_2/hexane mixtures to yield the reduced or so-called sp^3 forms[8] of the respective macrocycles. Air oxidation of these ligands in the presence of the appropriate metal ion (Cd(II), Zn(II), or In(III), as nitrate salts) was then carried out in the usual way[2] to give, after purification by column chromatography (silica gel, $CHCl_3/CH_3OH$ eluent, 1.0:0.1 v/v), pure samples of the new texaphyrin complexes in overall yields of 15–30%.

The $[(CNTXP)CD]^+$, $[(PNTXP)Cd]^+$, and $[(NPTXP)Cd^+$ complexes were synthesized with essentially the same procedure. Here, however, either diaminomaleonitrile or the appropriate aromatic diamine were used in the place of the derivatized diaminobenzene in the initial condensation. Following the oxidative metal insertion and chromatographic purification as above, the complexes were again isolated in yields ranging from 15 to 30%.

Cadmium(II) Complex of 4,5,9,24-Tetraethyl-16-methoxy-10,23-dimethyl-13,20,25,26,27-pentaazapentacyclo[20.2.1.1^{3,6}.1^{8,11}.0^{14,19}]heptacosa-1,3,5,7,9,11(27),12,14,16,18,20,22(25),23-tridecaene ($[(4\text{-}OCH_3TXP)Cd]^+$). ^1H NMR (CD_3OD): δ 1.67–1.72 (12 H, m, CH_2CH_3), 3.23 (3, s, pyrr–CH_3), 3.27 (3 H, s, pyrr–CH_3), 3.64–3.69 (8 H, m, CH_2CH_3), 4.42 (3 H, s, Ph–OCH_3), 8.13–8.17 (1 H, m, Ph H), 9.33 (1 H, m, Ph H), 9.49 (1 H, s, $(pyrr)_2$–CH), 9.52 (1 H, s, $(pyrr)_2$–CH), 9.88–9.91 (1 H, m, Ph H), 11.74–11.85 (2 H, m, CH=N). UV/vis (CH_2Cl_2) [λ_{max}, nm (log ϵ)]: 326.5 (4.38), 457 (4.73), 696 (3.85), 753.5 (4.35). FAB MS, M^+: *m/e* 631 (for ^{113}Cd). HR MS, M^+: *m/e* 628.1973 (calc for $C_{33}H_{36}N_5O^{110}Cd$, *m/e* 628.1950).

Cadmium(II) Complex of 4,5,9,24-Tetraethyl-10,16,17,23-tetramethyl-13,20,25,26,27-pentaazapentacyclo[20.2.1.1^{3,6}.1^{8,11}.0^{14,19}]heptacosa-1,3,5,7,9,11(27),12,14,16,18,20,22(25),23-tridecaene ($[(4,5\text{-}DMTXP)Cd]^+$). ^1H NMR ($CDCl_3$): δ 1.64–1.71 (12 H, m, CH_2CH_3), 2.90 (6 H, s, Ph–CH_3), 3.11 (6 H, s, pyrr–CH_3), 3.54–3.58 (8 H, m,

(1) (a) Sessler, J. L.; Murai, T.; Cyr, M. *Comments Inorg. Chem.* **1988**, *7*, 333. (b) Sessler, J. L.; Johnson, M. R.; Lynch, V. *J. Org. Chem.* **1987**, *52*, 4394.
(2) Sessler, J. L.; Murai, T.; Lynch, V.; Cyr, M. *J. Am. Chem. Soc.* **1988**, *110*, 5586.
(3) Harriman, A.; Maiya, B. G.; Murai, T.; Hemmi, G.; Sessler, J. L.; Mallouk, T. E. *J. Chem. Soc., Chem. Commun.* **1989**, 314.
(4) Regev, A.; Berman, A.; Levanon, H.; Murai, T.; Sessler, J. L. *Chem. Phys. Lett.* **1989**, *160*, 401.
(5) Maiya, B. G.; Harriman, A.; Murai, T.; Hemmi, G.; Sessler, J. L.; Mallouk, T. E. *J. Phys. Chem.* **1989**, *93*, 8111.
(6) Kreimer-Birnbaum, M. *Semin. Hematol.* **1989**, *26*, 157.
(7) Judy, M. M.; Boriack, R. L.; Matthews, J. L.; Sessler, J. L.; Hemmi, G. Abstracts of the 18th Annual Meeting of the American Society for Photobiology, Vancouver, Canada, June 1990.

(8) The designation "sp^3 form of the macrocycle" refers to reduced form of the texaphyrin ligand in which the meso-type carbon atoms are fully saturated and are sp^3-hybridized (see refs 1b and 2).

0020-1669/90/1329-3738$02.50/0

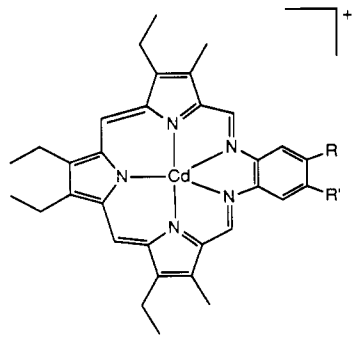

R= OCH_3	R'= H	$[(4\text{-}OCH_3TXP)Cd]^+$
R= CH_3	R'= CH_3	$[(4,5\text{-}DMTXP)Cd]^+$
R= CH_3	R'= H	$[(4\text{-}CH_3TXP)Cd]^+$
R= H	R'= H	$[(TXP)Cd]^+$
R= Cl	R'= H	$[(4\text{-}ClTXP)Cd]^+$
R= CO_2H	R'= H	$[(4\text{-}CO_2HTXP)Cd]^+$
R= NO_2	R'= H	$[(4\text{-}NO_2TXP)Cd]^+$

Figure 1. Structures of substituted *o*-phenylenediamine-derived cadmium(II) texaphyrins.

CH_2CH_3), 9.22 (2 H, s, Ph H), 9.34 (2 H, s, $(pyrr)_2$–CH), 11.30 (2 H, m, CH=N). UV/vis (CH_2Cl_2) [λ_{max}, nm (log ϵ)]: 323.5 (4.44), 448 (4.82), 697.5 (3.97), 7.58 (4.57). FAB MS, M^+: *m/e* 628 (for ^{112}Cd). HR MS, M^+: *m/e* 626.2136 (calc for $C_{34}H_{38}N_5{}^{110}Cd$, *m/e* 626.2157).

Cadmium(II) Complex of 4,5,9,24-Tetraethyl-10,16,23-trimethyl-13,20,25,26,27-pentaazapentacyclo[20.2.1.1^{3,6}.1^{8,11}.0^{14,19}]heptacosa-1,3,5,7,9,11(27),12,14,16,18,20,22(25),23-tridecaene ([(4-CH_3TXP)Cd]$^+$). ^1H NMR ($CDCl_3$): δ 1.61–1.70 (12 H, m, CH_2CH_3), 2.94 (3 H, s, Ph–CH_3), 2.95 (6 H, s, pyrr–CH_3), 3.44–3.55 (8 H, m, CH_2CH_3), 8.00–8.03 (1 H, m, Ph H), 8.95 (1 H, s, Ph H), 9.06–9.09 (1 H, m, Ph H), 9.16 (2 H, s, $(pyrr)_2$–CH), 10.89–10.90 (2 H, m, CH=N). FAB MS, M^+: *m/e* 616 (for ^{114}Cd). UV/vis (CH_2Cl_2) [λ_{max}, nm (log ϵ)]: 323 (4.45), 427 (4.78), 701 (3.95), 7.62 (4.55). HR MS, M^+: *m/e* 612.1973 (calc for $C_{33}H_{36}N_5{}^{110}Cd$, *m/e* 612.2001).

Cadmium(II) Complex of 16-Chloro-4,5,9,24-tetraethyl-10,23-dimethyl-13,20,25,26,27-pentaazapentacyclo[20.2.1.1^{3,6}.1^{8,11}.0^{14,19}]heptacosa-1,3,5,7,9,11(27),12,14,16,18,20,22(25),23-tridecaene ([(4-ClTXP)Cd]$^+$). ^1H NMR (CD_3OD): δ 1.65 – 1.70 (12 H, m, CH_2CH_3), 3.18 (6 H, s, pyrr–CH_3), 3.57–3.67 (8 H, m, CH_2CH_3), 8.43–8.46 (1 H, m, Ph H), 9.43 (2 H, s, $(pyrr)_2$–CH), 9.86–98.89 (1 H, m, Ph H), 9.96 (1 H, s, Ph H), 11.74 (2 H, m, CH=N). UV/vis (CH_2Cl_2) [λ_{max}, nm (log ϵ)]: 331.5 (4.40), 429 (4.65), 707.5 (3.77), 773 (4.32). FAB MS, M^+: *m/e* 636 (for ^{114}Cd). HR MS, M+: *m/e* 632.1424 (calc for $C_{32}H_{33}N_5{}^{35}Cl^{110}Cd$, *m/e* 632.1454).

Cadmium(II) Complex of 4,5,9,24-Tetraethyl-10,23-dimethyl-16-nitro-13,20,25,26,27-pentaazapentacyclo[20.2.1.1^{3,6}.1^{8,11}.0^{14,19}]heptacosa-1,3,5,7,9,11(27),12,14,16,18,20,22(25),23-tridecaene ([(4-NO_2TXP)Cd]$^+$). ^1H NMR (CD_3OD): δ 1.64–1.69 (12 H, m, CH_2CH_3), 3.18 (6 H, m, pyrr–CH_3), 3.54–3.66 (8 H, m, CH_2CH_3), 9.19–9.23 (1 H, m, Ph H), 9.40 (2 H, br, $(pyrr)_2$–CH), 10.01 (1 H, m, Ph H), 10.73 (1 H, br, Ph H), 11.76–11.83 (2 H, m, CH=N). UV/vis (CH_2Cl_2) [λ_{max}, nm (log ϵ)]: 440 (4.66), 739 (3.90), 797 (4.35). FAB MS, M^+: *m/e* 647 (calc for $C_{32}H_{33}N_6O_2{}^{114}Cd$, *m/e* 647).

Cadmium(II) Complex of 16-Carboxy-4,5,9,24-tetraethyl-10,23-dimethyl-13,20,25,26,27-pentaazapentacyclo[20.2.1.1^{3,6}.1^{8,11}.0^{14,19}]heptacosa-1,3,5,7,9,11(27),12,14,16,18,20,22(25),23-tridecaene ([(4-CO_2HXTP)Cd]$^+$). ^1H NMR (CD_3OD): δ 1.64–1.69 (12 H, m, CH_2CH_3), 3.18 (6 H, s, pyrr–CH_3), 3.55–3.65 (8 H, m, CH_2CH_3), 9.01–9.04 (1 H, m, Ph H), 9.38–9.39 (2 H, m, $(pyrr)_2$–CH), 9.90–9.93 (1 H, m, Ph H), 10.46 (1 H, s, Ph H), 11.74 (2 H, m, CH=N). UV/vis (CH_2Cl_2) [λ_{max}, nm (log ϵ)]: 335 (4.28), 4.30 (4.49(, 685 (sh), 782 (4.09). FAB MS, M^+: *m/e* 646 (for ^{114}Cd). HR MS, M^+: *m/e* 642.1724 (calc for $C_{33}H_{34}N_5O_2{}^{110}Cd$, *m/e* 642.1742).

Cadmium(II) Complex of 14,15-Dicyano-4,5,9,20-tetraethyl-10,19-dimethyl-13,16,21,22,23-pentaazatetracyclo[16.2.1.1^{3,6}.1^{8,11}]tricosa-1,3,5,7,9,11(23),12,14,16,18(21),19-undecaene ([CNTXP)Cd]$^+$). ^1H NMR ($CDCl_3$): δ 1.84–1.94 (12 H, m, CH_2CH_3), 3.36 (6 H, s, pyrr–CH_3), 3.98 (8 H, m, CH_2CH_3), 10.23 (2 H, s, $(pyrr)_2$–CH), 11.29 (2 H, m, CH=N). UV/vis ($CHCl_3$) [λ_{max}, nm, (log ϵ)]: 306 (4.39), 416 (4.82), 454 (sh), 600 (4.01), 635 (3.89), 692 (4.26). FAB MS, M^+: *m/e* 602 (for ^{114}Cd). HR MS, M^+: *m/e* 598.1569 (calc for $C_{30}H_{30}N_7{}^{110}Cd$, *m/e* 598.1592).

Cadmium(II) Complex of 4,5,9,28-Tetraethyl-10,27-dimethyl-13,24,29,30,31-pentaazahexaacyclo[24.2.1.1^{3,6}.1^{8,11}.0^{14,23}.0^{16,21}]hentriaconta-1,3,5,7,9,11(31),12,14(23),15,17,19,21,24,26(29),27-pentadecaene ([(NPTXP)Cd]$^+$). ^1H NMR (CD_3OD): δ 1.49–1.56 (12 H, m, CH_2CH_3), 2.94 (6 H, s, pyrr–CH_3), 3.25–3.38 (m, CH_2CH_3 + solvent), 7.94–7.97 (2 H, m, naphthyl H), 8.62–8.65 (2 H, m, naphthyl H), 8.67 (2 H, s, naphthyl H), 9.99 (2 H, s, $(pyrr)_2$–CH), 11.10–11.17 (2 H, m, CH=N). UV/vis (CH_2Cl_2) [λ_{max}, nm (log ϵ)]: 341 (4.28), 444 (4.76), 783 (3.98), 864 (4.39). FAB MS, M^+: *m/e* 652 (for ^{114}Cd). HR MS, M^+: *m/e* 648.2018 (calc for $C_{36}H_{36}N_5{}^{110}Cd$, *m/e* 648.2001).

Cadmium(II) Complex of 4,5,9,32-Tetraethyl-10,31-dimethyl-13,28,33,34,35-pentaazaheptacyclo[28.2.1.1^{3,6}.1^{8,11}.0^{14,27}.0^{15,20}.0^{21,26}]pentatriaconta-1,3,5,7,9,11(35),12,14(27),15(20),16,18,21(26),22,24,28,30-(33),31)-heptadecaene ([(PNTXP)Cd]$^+$). ^1H NMR (CD_3OD): δ 1.78–1.85 (12 H, m, CH_2CH_3), 3.37 (6 H, s, pyrr–CH_3), 3.85–3.92 (8 H, m, CH_2CH_3), 8.09–8.12 (4 H, m, phenanthyl H), 9.20–9.23 (2 H, m, phenanthyl H), 9.78–9.81 (2 H, m, phenanthyl H), 9.96 (2 H, s, $(pyrr)_2$–CH), 12.41 (2 H, m, CH=N). UV/vis (CH_2Cl_2) [λ_{max}, nm (log ϵ)]: 416 (4.42), 489 (4.84), 732 (4.18). FAB MS, M^+: *m/e* 702 (for ^{114}Cd). HR MS, M^+: *m/e* 701.2191 (calc for $C_{40}H_{38}N_5{}^{113}Cd$, *m/e* 701.2171).

(b) Methods. UV/visible spectra were taken on a Beckman Model DU-7 spectrophotometer. Cyclic voltammetric measurements were performed under an argon atmosphere with a conventional three-electrode system. The working electrode was a platinum button (area ~0.3 cm^2), and a platinum wire was used as a counter electrode. A saturated calomel electrode (SCE) was used as the reference electrode and was separated from the bulk solution by a fritted glass bridge that contained the solvent and the supporting electrolyte. A Pine Instruments Co. Model RDE-4 potentiostat/galvanostat was used to control the potential. Current–voltage curves were recorded on a Kipp & Zonen Model BD-90 recorder. All potentials are reported with respect to SCE and are uncorrected for *iR* drop and liquid-junction potentials. These effects are estimated to introduce errors of ≤10 mV in the reported peak potentials. Under these conditions a reversible oxidation peak at (0.47 ± 0.04) vs SCE was observed for the ferrocene/ferrocenium (Fc/Fc^+) couple in CH_2Cl_2, 0.1 M $(TBA)ClO_4$.

All electrochemical and spectral experiments were performed at 23 ± 2 °C, unless otherwise specified.

Results and Discussion

UV/Visible Spectra. Figures 3–5 show the UV/visible spectra of several representative cadmium(II) texaphyrin type complexes. The spectra of two substituted *o*-phenylenediamine-derived systems, $[(4\text{-}OCH_3TXP)Cd]^+$ and $[(4\text{-}NO_2TXP)Cd]^+$, are shown

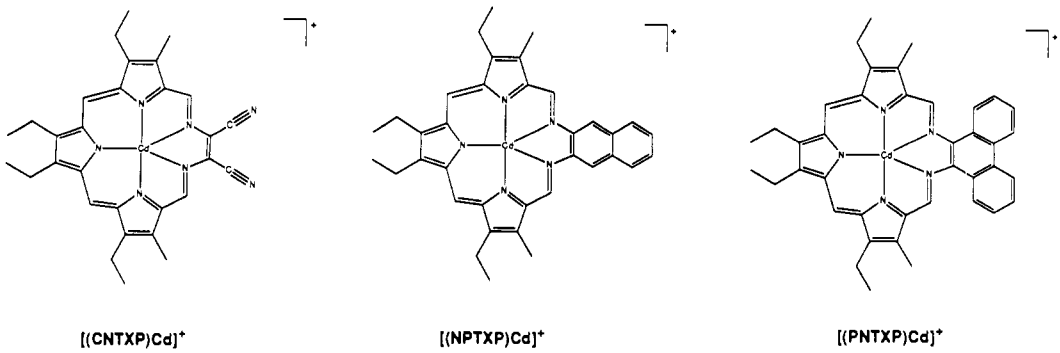

$[(CNTXP)Cd]^+$ $[(NPTXP)Cd]^+$ $[(PNTXP)Cd]^+$

Figure 2. Structures of $[(CNTXP)Cd]^+$, $[(NPTXP)Cd]^+$, and $[(PNTXP)Cd]^+$.

Table I. UV/Visible and Electrochemical Data for Various Texaphyrin Complexes[a]

	UV/vis data				redox data, V			
	Soret		Q		oxidn	redn[c]		
compd	λ_{max}, nm	log ϵ	λ_{max}, nm	log ϵ	$E_{1/2}$(ox)	$-E_{pc}$	$-E_{pa}$	$-E_{1/2}$(red, py)
[(4-OCH_3TXP)Cd]$^+$	457[d]	4.73	754	4.35	1.09	0.39	0.31	0.45
[(4,5-DMTXP)Cd]$^+$[e]	448[d]	4.82	758	4.57	1.05	0.45	0.35	0.47
[(4-CH_3TXP)Cd]$^+$	427	4.78	762	4.55	1.10	0.45	0.31	0.43
[(TXP)Cd]$^+$	425[f]	4.92	770[f]	4.70	1.09	0.36	0.26	0.40
[(4-ClTXP)Cd]$^+$	429	4.65	773	4.32	1.14	0.36	0.28	0.37
[(4-CO_2HTXP)Cd]$^+$	430	4.49	782	4.09	1.13	0.35	*g*	0.37
[(4-NO_2TXP)Cd]$^+$	440	4.66	797	4.35	1.17	0.17	0.08	0.23
[(TXP)Zn]$^+$	409[f]	4.62	754[f]	4.33	1.08			0.42
[(4-CO_2HTXP)In]$^{2+}$	436		769		*h*			0.30
[(CNTXP)Cd]$^+$	417[f]	4.82	692[f]	4.26	>1.8[i]	0.22	*g*	0.18
[(PNTXP)Cd]$^+$	489	4.84	733	4.18	1.25	0.36	*g*	0.41
[(NPTXP)Cd]$^+$	440	4.76	864	4.39	1.03	0.24	0.18	0.28

[a] Unless otherwise indicated, the counteranion was always nitrate and the measurements were carried out in CH_2Cl_2 (absorption studies) or CH_2Cl_2 containing 0.1 M (TBA)ClO_4 (electrochemical measurements). Estimated error limits: peak maxima, ±1 nm; redox potentials, ±10 mV. [b] Half-wave potential for reversible, one-electron oxidation of complexes in the absence of pyridine. [c] E_{pa} and E_{pc} refer respectively to cathodic and anodic peak potentials for the quasi-reversible reduction in the absence of added pyridine. $E_{1/2}$(red, py) is the half-wave potential for the reversible one-electron reduction of the texaphyrins in the presence of ca. 10^{-2} M pyridine. [d] For both complexes a major shoulder at ca. 425 nm was also observed. The wavelengths quoted refer, however, to the maximum intensity positions. [e] DM in [(4,5-DMTXP)Cd]$^+$ is the abbreviation for "dimethyl" (see Figure 1). [f] In $CHCl_3$. [g] No peaks were observed in these cases. [h] Complex was sparingly soluble in CH_2Cl_2 + (TBA)ClO_4, and hence the oxidation reaction could not be monitored. In the presence of pyridine, the complex was sufficiently soluble, but no peak was observed in the anodic potential range 0–1 V. [i] No peak was observed in the potential range 0–1.8 V (see text).

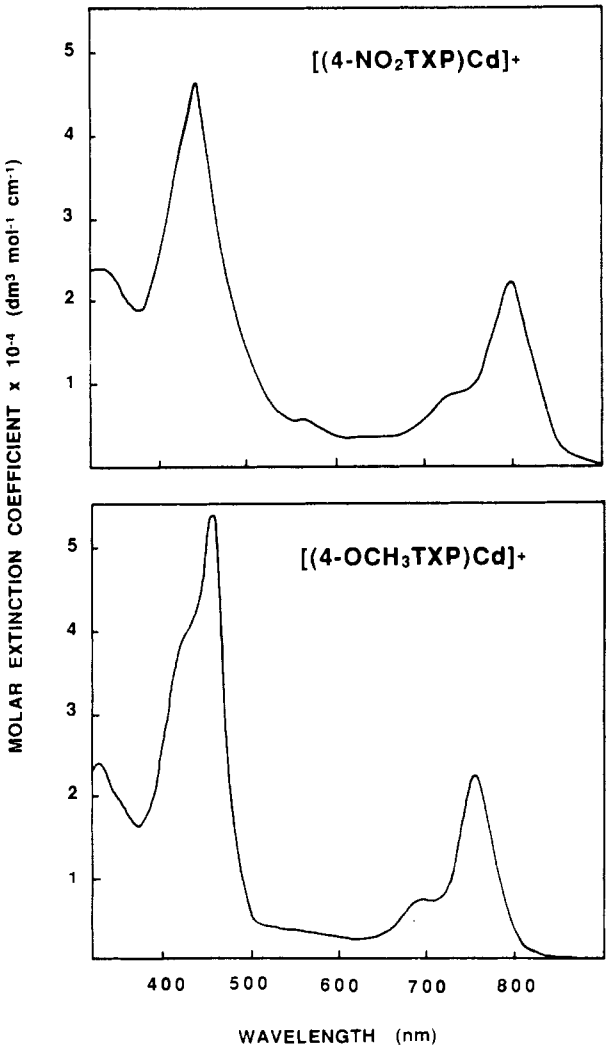

Figure 3. UV/visible absorption spectra of two representative *o*-phenylenediamine-derived cadmium(II) texaphyrins in dichloromethane.

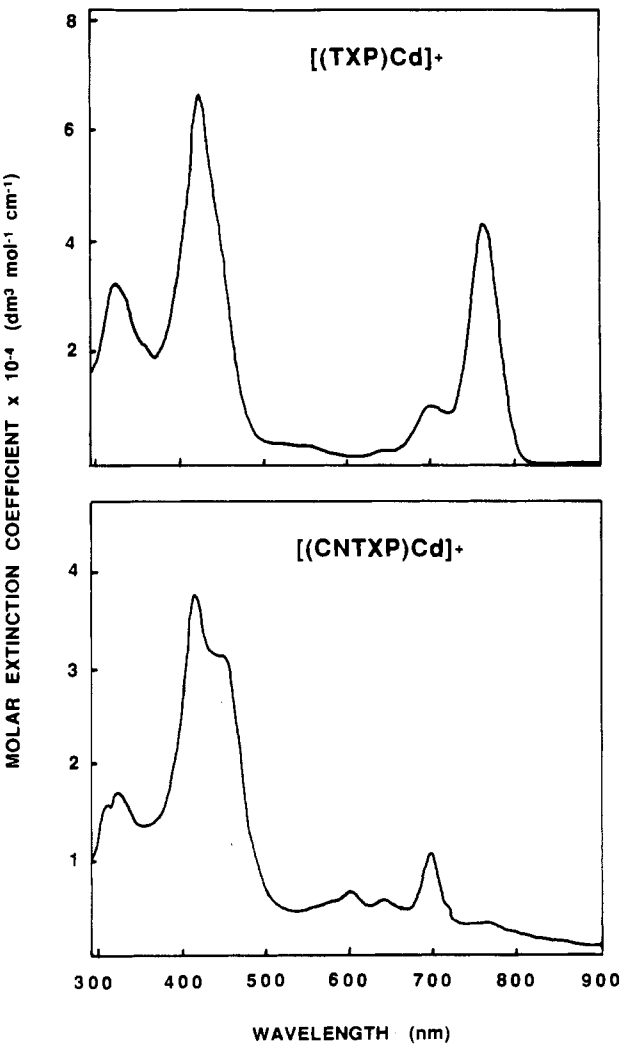

Figure 4. UV/visible absorption spectra of the unsubstituted cadmium(II) tetraphyrin, [(TXP)Cd]$^+$, and the diaminomaleonitrile-derived system, [(CNTXP)Cd]$^+$, in chloroform.

in Figure 3, the spectrum of the unsubstituted texaphyrin system, [(TXP)Cd]$^+$, and the diaminomalionitrile-derived complex, [(CNTXP)Cd]$^+$, are shown in Figure 4, and the UV/visible spectra of the naphthalene and phenanthrene-based materials, [(NPTXP)Cd]$^+$ and [(PNTXP)Cd]$^+$, are shown in Figure 5. Spectral data for these protypical complexes and related systems are summarized in Table I.

As seen in Figures 3–5, the cadmium(II) texaphyrin type complexes all display characteristic Soret- and Q-type bands (a

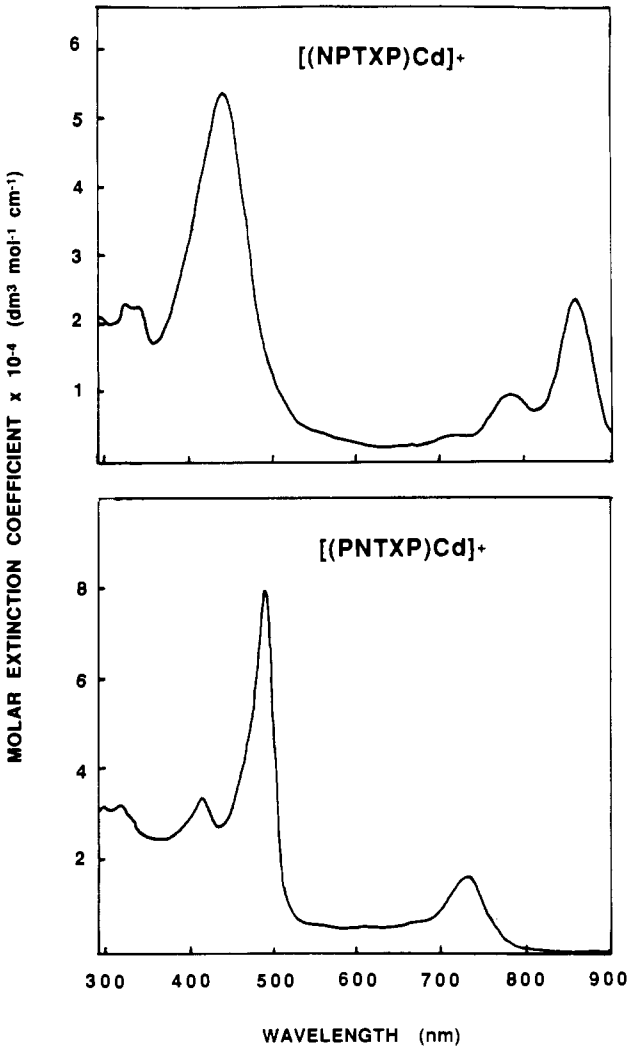

Figure 5. UV/visible absorption spectra of the naphthalene- and phenanthrene-based cadmium(II) tetraphyrin type complexes, [(NPTXP)Cd]$^+$ and [(PNTXP)Cd]$^+$, in dichloromethane.

terminology based on porphyrin absorption spectra[9]). In the case of the *o*-phenylenediamine-derived complexes, which will be considered first, the peak maximum of the Soret-type band varies from 425 to 457 nm, while that of the most intense Q-type band varies from 754 to 797 nm. Here, the actual position of the Q-type band maximum depends on the substituent R and on the solvent: Electron-donating substituents on the phenyl ring shift the peak maximum to the higher energy side and electron-withdrawing substituents shift the peak maximum to the lower energy side of the spectrum, whereas changing from CH_2Cl_2 to CH_3OH effects a slight ($\leq$10 nm) hypsochromic shift in this same peak maximum.

In the case of metalloporphyrins, it is well established that the lowest energy absorption band (i.e., the Q band) maximum correlates with the HOMO–LUMO energy gap of the macrocycle.[10,11] On the basis of the similarity in the electronic absorption spectra of porphyrins and texaphyrins, it is reasonable to expect that this relationship will hold for texaphyrins also. Thus, a variation of the Q-type band maxima observed for the substituted *o*-phenylenediamine-derived texaphyrins is a manifestation of the modulation of HOMO–LUMO energy gap that is brought about by the change of substituents at the periphery of the macrocyclic π-ring. Support for this hypothesis comes from electrochemical data obtained with these complexes (see below).

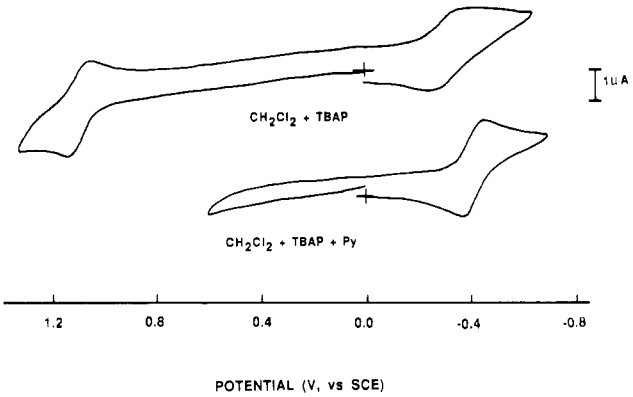

Figure 6. Cyclic voltammograms of [(TXP)Cd]$^+$ in CH_2Cl_2, 0.1 M $(TBA)ClO_4$ with and without added pyridine (10^{-2} M). Scan rate = 100 mV s^{-1}.

The absorption data in Table I and the spectra reproduced in Figures 4 and 5 also suggest that a change in the extent of aromaticity of the texaphyrins affects their absorption spectra. For example, [(CNTXP)Cd]$^+$, being an 18-π-electron system, has its Q-type band located at higher energy, compared to the 22-π-electron *o*-phenylenediamine-derived complexes (compare Figures 3 and 4). On the other hand, [(NPTXP)Cd]$^+$, a naphthannelated 18-π-electron macrocycle (an overall 26-π-electron system!) has a corresponding band at 865 nm that is extremely (about 100 nm) red-shifted, compared to the Q-band position of the benzannelated texaphyrin, [(TXP)Cd]$^+$ (compare Figures 4 and 5). The case of [(PNTXP)Cd]$^+$ (Figure 5) is slightly different in that although it has three fused benzene rings and therefore a larger aromatic π-system, molecular models (CPK) show that this system is strained and that the phenanthryl ring is not coplanar with the rest of the atoms in the macrocyclic ring. Hence, as a consequence of restricted π-conjugation, this complex has its Q-type absorption peak located at wavelengths as short as 730 nm.

Collectively, these spectral results suggest that derivatization of this pentadentate macrocycle is synthetically simple and that fine-tuning of the lowest energy absorption band maximum is facile for texaphyrins, relative to porphyrins and related tetrapyrrolic complexes. The change in the absorption features of tetraaryl- or octaethylporphyrins derived at their meso or β-pyrrole positions is not as dramatic as that seen here for analogously substituted cadmium(II) texaphyrins. For example, introduction of a nitro group at the β-pyrrole[12] or the *meso*-phenyl[13] positions of tetraphenylporphyrins shifts their Q-band absorption maxima by only 2–15 nm. In contrast, [(4-NO_2TXP)Cd]$^+$ absorbs about 30 nm to the red of the unsubstituted texaphyrin [(TXP)Cd]$^+$. The change in the Q-type band maxima observed in going from [(TXP)Cd]$^+$ to [(NPTXP)Cd]$^+$ is similar ($\sim$100 nm) to that observed for the change in Q-band maxima in going from a metallophthalocyanine to a metallonaphthalocyanine.[6,14]

Redox Potentials. [(TXP)Cd]$^+$. Figure 6 shows the cyclic voltammogram of [(TXP)Cd]$^+NO_3^-$ in CH_2Cl_2 containing 0.1 M tetra-*n*-butylammonium perchlorate ($(TBA)ClO_4$). The complex undergoes a reversible, diffusion-controlled one-electron oxidation[15,16] at (1.09 $\pm$ 0.1) V. For this oxidation, $|E_{p_a} - E_{\infty p_c}|$ = (60 $\pm$ 5) mV, $i_{p_a}/i_{p_c} \sim$ 0.9–1.0, and $i_p/v^{1/2}$ is constant with scan rate (v) over the range 50–500 mV s^{-1}. Under the same conditions, a cathodic potential scan shows, however, a quasi-reversible reduction process with $E_{p_c} \doteq -(0.36 \pm 0.04)$ V and $E_{p_a} = -(0.26 \pm 0.03)$ V. This process is characterized by $|E_{p_a} - E_{p_c}|$ of 80–130

(9) Gouterman, M. In *The Porphyrins*; Dolphin, D., Ed.; Academic Press: New York, 1979; Vol. 3, Chapter 1.
(10) Fuhrop, J.-H.; Kadish, K. M.; Davis, D. G. *J. Am. Chem. Soc.* **1973**, *95*, 5140.
(11) Zerner, M.; Gouterman, M. *Theor. Chim. Acta* **1966**, *4*, 44.
(12) Baldwin, J. E.; Maxwell, J. C.; DeBernardis, J. *Tetrahedron* **1982**, *38*, 685.
(13) Collman, J. P.; Gagne, R. R.; Reed, C. A.; Halbert, T. R.; Lang, G.; Robinson, W. T. *J. Am. Chem. Soc.* **1975**, *97*, 1427.
(14) Ford, W. E.; Rihter, B. D.; Kenney, M. E.; Rodgers, M. A. J. *Photochem. Photobiol.* **1989**, *50*, 277.
(15) Bard, A. J.; Faulkner, L. R. *Electrochemical Methods: Fundamentals and applications*; Wiley Interscience: New York, 1980.
(16) Nicholson, R. S.; Shain, I. *Anal. Chem.* **1964**, *36*, 706.

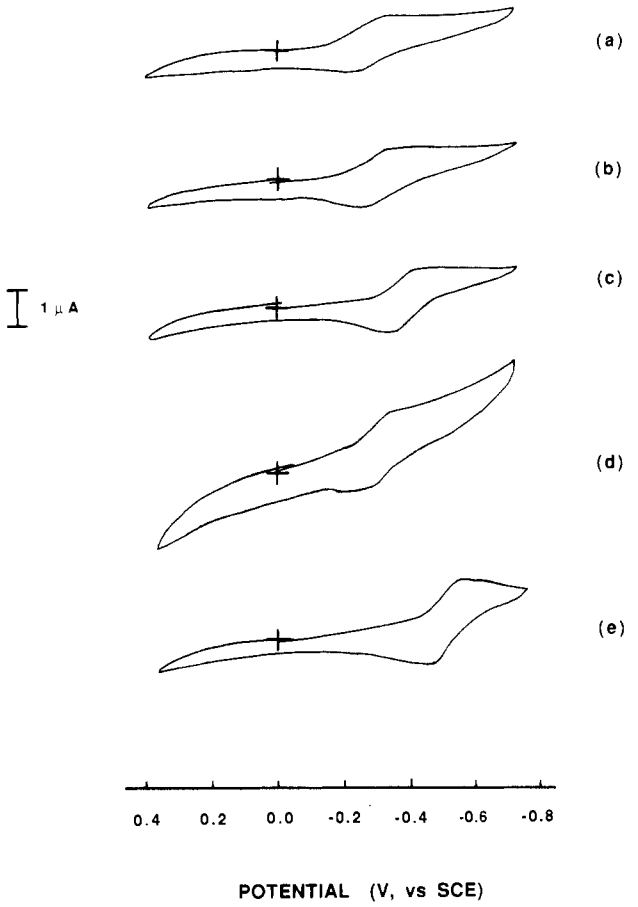

Figure 7. Cyclic voltammograms of $[(TXP)Cd]^+NO_3^-$ under various solution conditions: (a) CH_2Cl_2, 0.1 M $(TBA)ClO_4$; (b) CH_2Cl_2, 0.1 M $(TBA)ClO_4$ + 10^{-2} M 2,6-lutidine; (c) CH_2Cl_2, 0.1 M $(TBA)ClO_4$ + 10^{-2} M pyridine; (d) pyridine, 0.1 M $(TBA)ClO_4$; (e) CH_2Cl_2, 0.1 M $(TBA)ClO_4$ + 10^{-2} M (TBA)Cl. In all cases, the scan rate was 100 mV s^{-1}.

mV and i_{p_a}/i_{p_c} of ca. 0.5–0.8 at scan rates of 20–500 mV s^{-1}. Thus, the redox behavior of $[(TXP)Cd]^+NO_3^-$ in CH_2Cl_2, 0.1 M $(TBA)ClO_4$ is similar to that reported earlier[5] for the complex in CH_3CN, 0.1 M $(TBA)BF_4$. By analogy, the electrode reactions can be represented as follows:

$$[(TXP)Cd]^+ \rightleftarrows [(TXP)Cd]^{2+} + e^- \quad (1)$$

$$[(TXP)Cd]^+ + e^- \rightleftarrows [(TXP)Cd]^0 \quad (2)$$

It was found that neither an increase in the potential scan rate, up to 500 mV s^{-1}, or a decrease in temperature, to ca. −10 °C, made the reduction process electrochemically reversible for $[(TXP)Cd]^+NO_3^-$. The quasi-reversibility of the reduction peak of this highly aromatic complex is somewhat surprising, and in order to understand this, a series of exploratory experiments[17] were performed, the results of which are shown in Figure 7. The reduction of $[(TXP)Cd]^+$ remains quasi-reversible upon addition of 10^{-2} M (or more) 2,6-lutidine (E_{p_c} = −0.37 V, E_{p_a} = −0.27 V). However, in the presence of 10^{-2} M pyridine, or in neat pyridine, the process becomes reversible, and under these conditions, $|E_{p_c} - E_{p_a}| = (60 \pm 5)$ mV, $i_{p_c}/i_{p_a} \simeq 1$, and $i_p/v^{1/2}$ is constant with scan rate. $E_{1/2}$ is −(0.40 ± 0.04) V in CH_2Cl_2 containing 10^{-2} M pyridine and is −(0.38 ± 0.04) V in neat pyridine. Figure 7 also shows that addition of 10^{-2} M *tetra-n*-butylammonium chloride ((TBA)Cl) to CH_2Cl_2 solutions of $[(TXP)Cd]^+$ containing 0.1 M $(TBA)Cl)_4$ makes the reduction electrochemically reversible, and in this case $E_{1/2}$ is shifted to −(0.49 ± 0.05) V.

(17) Liquid-junction potentials are likely to introduce a larger uncertainty in the half-wave potentials determined in solutions containing both CH_2Cl_2 and the added ligand (i.e. pyridine, Cl^-, NO_3^-, or 2,6-lutidine).

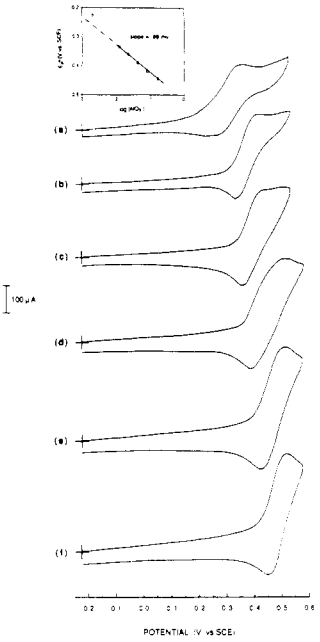

Figure 8. Cyclic voltammograms of 2 mM $[(TXP)Cd]^+$ in CH_2Cl_2, 0.1 M tetrabutylammonium perchlorate with added tetrabutylammonium nitrate. Nitrate concentrations were (a) 2 mM, (b) 12 mM, (c) 22 mM, (d) 40 mM, (e) 80 mM, and (f) 160 mM. The scan rate was 50 mV s^{-1}. Inset shows a plot of anodic peak current vs log $[NO_3^-]$.

Bottomley and Kadish observed a similar change from quasi-reversible to reversible reduction upon addition of either tetra-*n*-butylammonium bromide ((TBA)Br) or a nitrogen base to iron porphyrin solutions in noncoordinating solvents.[18] They suggested that the quasi-reversible nature of the reduction peak is due to a loss of weakly bound porphyrin counterion (ClO_4^-) upon reduction in CH_2Cl_2, 0.1 M $(TBA)ClO_4$. They also suggested that, in the presence of strongly binding N_3^-, F^-, or nitrogen bases, this loss of counterion or ligand does not occur and the reduction is therefore electrochemically reversible.[19] We expect a similar mechanism to be operative for the reduction of $[(TXP)Cd]^+$. Specifically, we propose that loss of NO_3^- of ClO_4^- anion occurs upon addition of an electron to Cd(II) texaphyrin, resulting in quasi-reversibility for the reduction reaction in CH_2Cl_2, 0.1 M $(TBA)ClO_4$ (vida infa).

In the presence of strongly bound ligands such as Cl^- or pyridine, the reduction of $[(TXP)Cd]^+$ shows totally reversible behavior, as is the case for iron porphyrins under similar experimental conditions. Interestingly, the quasi-reversibility of the $[(TXP)Cd]^+$ reduction in the presence of essentially noncoordinating 2,6-lutidine is also consistent with this proposal.[20]

Further support for binding of pyridine to $[(TXP)Cd]^+$ complexes from ^1H NMR spectra of the complex in $CDCl_3$ containing various amounts of added pyridine.[21] Analysis of the spectra suggested that pyridine coordination to $[(TXP)Cd]^+$ does not occur in a discrete stepwise manner. In fact, it was possible to estimate only the apparent binding constants, K_1 = 1.6 M^{-1} (for formation of monopyridine adduct) and $K_1K_2 = (315 \pm 30)$ M^{-2} (formation of bispyridine adduct) with this method. In principle, it is possible to calculate the successive pyridine binding constants for the singly reduced complex (i.e. $[(TXP)Cd]^0$) from the cyclic voltammetric data.[15] However, the quasi-reversibility of this reduction in the absence of pyridine (eq 2) and the complexity of the pyridine

(18) Bottomley, L. A.; Kadish, K. M. *Inorg. Chem.* **1981**, *20*, 1348.
(19) Kadish, K. M.; Rhodes, R. K. *Inorg. Chem.* **1983**, *22*, 1090.
(20) In the case of iron porphyrins, reduction involves the metal center,[18] whereas the electron-transfer reaction almost certainly involves the ring redox orbitals with cadmium(II) texaphyrins. In spite of this difference, we believed that the same explanation holds for the quasi-reversibility of the reduction processes for both macrocycles in the presence and in the absence of 2,6-lutidine.
(21) Sessler, J. L.; Murai, T.; Lynch, V. *Inorg. Chem.* **1989**, *28*, 1333.

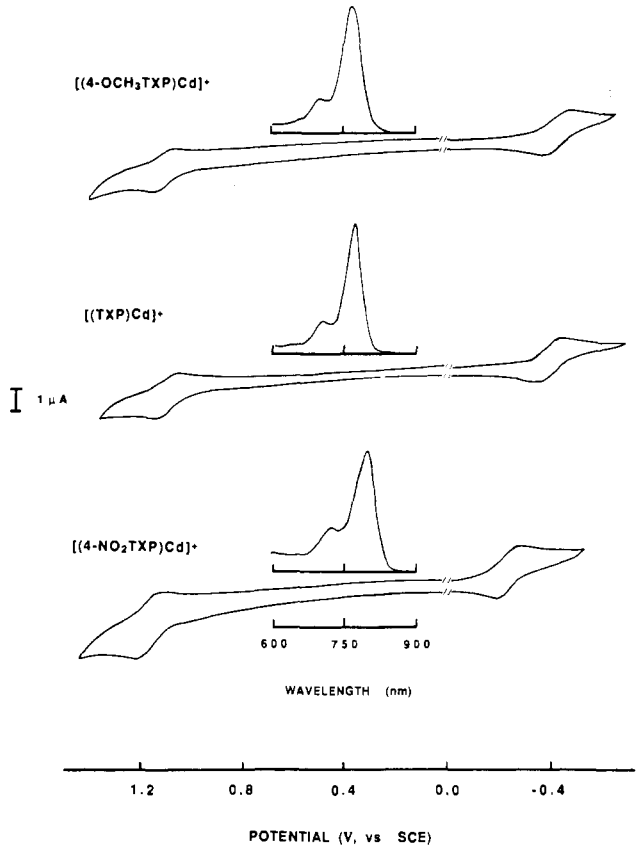

Figure 9. Cyclic voltammograms of $[(4\text{-}OCH_3TXP)Cd]^+$, $[(TXP)Cd]^+$, and $(4\text{-}NO_2TXP)Cd]^+$. The positive potential scan regions were run in CH_2Cl_2, 0.1 M $(TBA)ClO_4$, and the negative potential scan regions, in CH_2Cl_2, 0.1 M $(TBA)ClO_4$ containing $\sim 10^{-2}$ M pyridine. In each case, the scan rate was 100 mV s^{-1}. The inset shows the corresponding absorption spectra of the complexes in the Q-type band region.

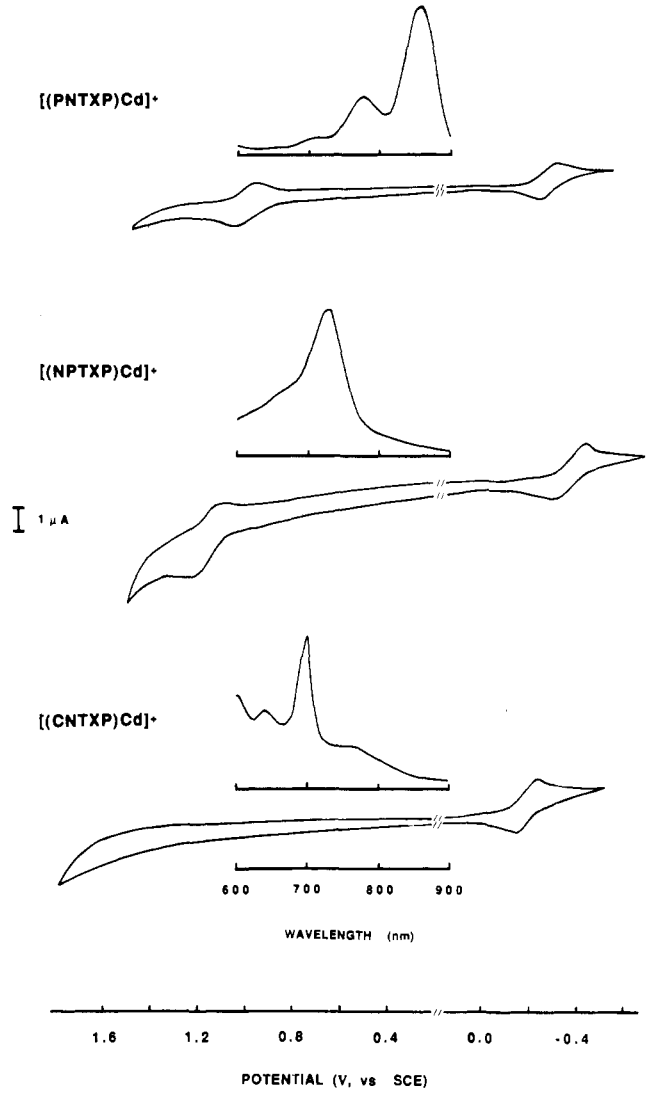

Figure 10. Cyclic voltammograms of $[(NPTXP)Cd]^+$, $[(PNTXP)Cd]^+$, and $[(CNTXP)Cd]^+$. The positive potential scan regions were run in CH_2Cl_2, 0.1 M $(TBA)ClO_4$, and the negative potential scan regions, in CH_2Cl_2, 0.1 M $(TBA)ClO_4$ containing $\sim 10^{-2}$ M pyridine; scan rate = 100 mV s^{-1}. The inset shows the corresponding absorption spectra of the complexes in the Q-type band region.

binding profile for $[(TXP)Cd]^+$ preclude a quantitative treatment for pyridine coordination of $[(TXP)Cd]^0$.

Cyclic voltammograms corresponding to the reduction and reoxidation of $[(TXP)Cd]^+$ in the presence of varying amounts of added tetrabutylammonium nitrate are shown in Figure 8. The effect of NO_3^- on the electrochemistry is similar to that of coordinating ligands such as pyridine; however, the change from irreversible to reversible behavior is gradual because of the smaller formation constants of the nitrate complexes. The shift to more negative potentials with increasing nitrate concentration is consistent with stronger binding of the latter to the oxidized form of the complex, relative to the reduced form, and the reversible shape of the waves in scan f suggests that, at high concentration, NO_3^- binds to both the oxidized and reduced forms. The inset in Figure 8 shows that the anodic peak current is linearly related to log $[NO_3^-]$ over a concentration range 12–160 mM. Interestingly, the slope of the line (−99 m) is intermediate between the −59 mV expected for binding of one nitrate ligand and −118 mV for binding of two nitrate ligands by the complex. It is likely that, in this concentration range, both forms are present and interconverting. From now-standard NMR experiments[21] carried out with similar solutions approximate binding constants were calculated for the oxidized form, $[(TXP)Cd]^+$: for this complex log $K_1 = 1.2 \pm 0.2$ and log $K_2 = 0.3 \pm 0.2$.

Cadmium(II) octaethylporphyrin, [Cd(OEP)], is an 18-π-electron system that is structurally related to the 22-π-electron $[(TXP)Cd]^+$. It is of interest to compare the redox chemistry of these two macrocycles. It has been reported that [Cd(OEP)] undergoes diffusion-controlled, reversible one-electron oxidation and reduction reactions at 0.55 V and −1.52 V, respectively.[22] Thus, the "expanded" porphyrin is more difficult to oxidize (by ca. 0.5 V) and is much easier to reduce (by ca. 1.2 V) than is [Cd(OEP)]. Moreover, the potential difference for oxidation and reduction of unsubstituted $[(TXP)Cd]^+$ (1.4 ± 0.2 V) is significantly smaller than the corresponding differences normally observed for metallooctaethylporphyrins (2.2 ± 0.2 V)[14] and metallophthalocyanines (1.7 ± 0.2 V).[23] As discussed earlier,[5] these differences may be ascribed to a greater degree of π-electron conjugation for the expanded porphyrin.

Substituted Cadmium Texaphyrins. The electrochemical redox potentials of the substituted *o*-phenylenediamine-derived texaphyrin complexes are listed in Table I. Representative cyclic voltammograms for $[(4\text{-}OCH_3TXP)Cd]^+$, $[(TXP)Cd]^+$, and $[(4\text{-}NO_2TXP(Cd)]^+$ are shown in Figure 9. As with the parent $[(TXP)Cd]^+$ complex, addition of pyridine or (TBA)Cl makes the reduction of these new, substituted texaphyrin complexes electrochemically reversible. The voltammograms of $[(CNTXP)Cd]^+$, $[(PNTXP)Cd]^+$, and $[(NPTXP)Cd]^+$, along with the accompanying Q-band spectra, are shown in Figure 10. Again, the anodic scans were run in the absence of pyridine, while the cathodic scans were run with 10^{-2} M added pyridine to ensure the reversibility of the reaction. Interestingly, $(CNTXP)Cd]^+$ could not be oxidized at potentials negative of +1.8 V (which is

(22) Davis, D. G. In *The Porphyrins*; Dolphin, D., Ed.; Academic Press: New York, 1979; Vol. 5, Part C, Chapter 4.

(23) Collins, G. C. S.; Schiffrin, D. J. *J. Electroanal. Chem. Interfacial Electrochem.* **1982**, *139*, 335.

the solvent breakdown limit under these conditions). Presumably this is a reflection of the highly electron withdrawing cyano groups.

In the case of porphyrins, it has been well established that both one-electron oxidation and reduction reactions involve principally ring-based orbitals. For the texaphyrin macrocycle, the similarities in the redox potentials of cadmium(II), zinc(II), and indium(III) complexes[24] (Table I) suggest that these electron-transfer reactions also involve primarily ring-centered orbitals. Oxidation involves abstraction of an electron from the HOMO of the complex, and the electron gained upon reduction is accommodated by the LUMO of the extended π-system. The substituents on the phenyl ring are expected to alter the energy of these frontier orbitals, depending on whether they are electron donating or electron withdrawing. Again, data obtained with these new texaphyrin derivatives can be compared with earlier work on porphyrins for which extensive data are available.

Systematic studies have been carried out on the electrochemistry of substituted tetraphenylporphyrins.[25] These studies have established that addition of electron-donating groups generally facilitates oxidation and hinders reduction at either the metal center or the porphyrin π-ring system. Electron-withdrawing substituents on the phenyl rings remove electron density from π-system, shifting the formal potentials for oxidation and reduction to more positive values. It should be noted, however, that in *meso*-tetraphenylporphyrin derivatives, the phenyl rings are almost perpendicular to the porphyrin π-plane. Redox tuning by substituents involves a change in porphyrin basicity, which is brought about by the σ-inductive effects of the substituents. On the other hand, electrochemical studies carried out with porphyrins in which the substituents are attached directly to the π-skeleton have shown the substituent effects on redox potentials reflect resonant interactions of the substituents and the porphyrin macrocycle.[26] In the texaphyrin series, the phenyl moiety is an intimate part of the macrocyclic π-system. Therefore, substitution at the inplane phenyl ring of the macrocycle directly perturbs the π-conjugation, and resonant interactions are possible between the substituent and the main macrocyclic frame, as with the β-substituted porphyrins. Table I shows that electron-donating substituents, such as methyl or methoxy, shift the reduction potentials to slightly more negative values, relative to unsubstituted [(TXP)Cd$^+$]. Similarly, electron-withdrawing groups such as Cl, CO_2H, and NO_2 induce positive shifts in the reduction potentials. The largest such shift (170 mV) is observed for NO_2, which is expected to have the greatest resonant coupling with the macrocyclic π-system. Texaphyrins with electron-withdrawing substituents are more difficult to oxidize than unsubstituted [(TXP)Cd]$^+$, but a similar trend is not strictly followed with electron-donor groups such as methyl and methoxy.

The inset in Figure 9 shows the Q-type band region absorption spectra of three representative *o*-phenylenediamine-derived texaphyrin complexes. From an analysis of the Q-band spectra of the compounds listed in Table I, we find a correlation between the absorption maxima and the absolute difference between the one-electron oxidation and reduction potentials ($E_{1/2}$(ox) − $E_{1/2}$(red)) of the substituted texaphyrins. This relation is shown in Figure 11.[27] The plot is roughly linear, although there is considerable scatter, and is reminiscent of a similar relationship found for free-base porphyrins and metalloporphyrins.[26] With β-substituted porphyrins, the lowest energy electronic absorption band, or HOMO–LUMO energy gap, and $|E_{1/2}(ox) - E_{1/2}(red)|$ are linearly related. The similar trend in the texaphyrin series can thus be explained in terms of a modulation of the HOMO–LUMO energy gap by the substituents; the extent of this modulation depends on the magnitude of the electron-donating or -withdrawing power and the number of attached substituents.[26] That the slope of the line in Figure 11 is less than 8×10^3 cm^{-1} V^{-1} indicates that either the reduction or oxidation is not completely localized on the macrocyclic ring; for example, for [(4-NO_2TXP)Cd]$^+$ (point 7 in Figure 11), it is reasonable that some electron density is localized on the nitro group upon reduction.

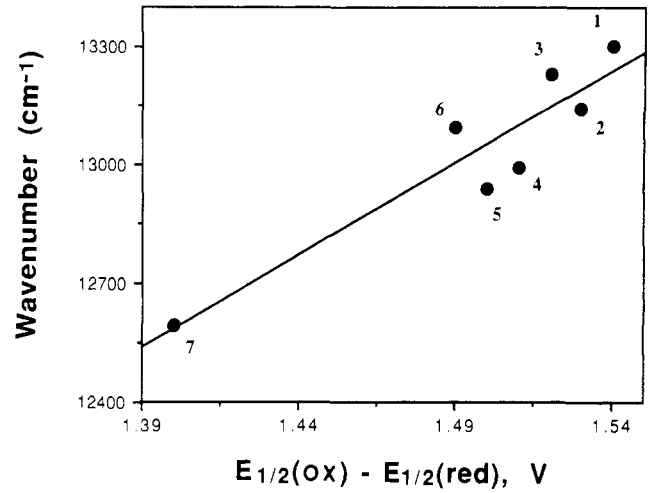

Figure 11. Plot of energies of the Q-type band maxima (wavenumber, cm^{-1}) vs the difference in potentials for first oxidation and reduction ($E_{1/2}$(ox) − $E_{1/2}$(red), V) of various texaphyrins: (1) [(4-OCH_3TXP)Cd]$^+$; (2) [(4,5-DMTXP)Cd]$^+$; (3) [(4-CH_3TXP)Cd]$^+$; (4) [(TXP)Cd]$^+$; (5) [(4-ClTXP)Cd]$^+$; (6) [(4-CO_2HTXP)Cd]$^+$; (7) [(4-NO_2TXP)Cd]$^+$. The correlation coefficient for the linear fit is 0.86.

A more general relationship between the electrochemical properties of these complexes and those of non-porphyrinic organic systems containing simple alternating double-bonded hydrocarbons can be conceived. It has been demonstrated that the redox potentials for a series of hydrocarbons with increasing π-electron density will vary linearly with the energy of their absorption band.[28] Spectral data from the cadmium(II) tetraphyrins fit well to such a relationship. The $E_{1/2}$ values for one-electron reductions of formally 22-π-electron macrocycles [(PNTXP)Cd]$^+$, [(TXP)Cd]$^+$, and [(NPTXP)Cd]$^+$ show one-to-one correspondence with their lowest energy absorption maxima. Although it should not be overinterpreted, this finding of linearity suggests that each texaphyrin complex can be accurately described as an aromatic entity.

Conclusions. In summary, absorption maxima and redox potentials of the texaphyrins reported in this study are influenced by the nature of substituents attached to the phenyl ring as well as by the extent of π-electron conjugation of the macrocycle. There is a linear relationship between energies of the Q-type band maximum and difference in the first oxidation and reduction potentials for texaphyrin complexes. This finding suggests that, as with the porphyrins, the Q-type band energies of the texaphyrins correspond to the relevant π-electron HOMO–LUMO energy gaps.

The Q-type band absorption maxima of the texaphyrins reported in this study vary between 692 and 864 nm. This large variability is potentially very useful in photosensitization applications. The absorption maxima of the texaphyrin family of photosensitizers correspond to the spectral reagions that are easily attained by the newer solid-state tunable laser sources, such as alexandrite (720–800 nm) and Ti–sapphire (700–950 nm), and by diode laser sources. Deliberate variation of the oxidation and reduction potentials as demonstrated here is relevant to the mechanistic

(24) The observed trend in the redox potentials of Zn(II), Cd(II), and In(III) complexes could reflect the presence of different substituents at the phenyl ring (i.e. H or CO_2H) and/or a possible difference in their net ring charges. Such trends have been observed previously with metalloporphyrins.

(25) Kadish, K. M. *Prog. Inorg. Chem.* **1986**, *34*, 435.

(26) Giraudeau, A.; Callot, H. J.; Gross, M. *Inorg. Chem.* **1979**, *18*, 201.

(27) The Q-band maxima used in plotting Figure 11 were measured in CH_2Cl_2 containing 0.1 M (TBA)ClO_4 and ca. 10^{-2} M pyridine. This was done in order to have a consistent set of conditions for both electrochemical and absorption spectral measurements. However, minimal spectral changes were found upon addition of (TBA)ClO_4 + pyridine to solutions of the same texaphyrin complexes in CH_2Cl_2 or CH_3OH. Also, even when spectral data obtained in CH_3OH were used in place of the data obtained in CH_2Cl_2 ((TBA)ClO_4 + pyridine), a plot of ν_Q (cm^{-1}) vs $E_{1/2}$(ox) − $E_{1/2}$(red) was linear with correlation of ca. 0.8.

(28) Heilbronner, E. Bock, H. *Das HMO-Modell und Seine Anwendung*; Verlag Chemie; Weinheim/Bergstrasse, Germany, 1968; Chapter 6.

aspects of photodynamic therapy (PDT). It is still not clear whether singlet molecular oxygen, O_2 (energy-transfer product, type II mechanism), superoxide radical, $O_2^{\bullet-}$ (electron-transfer product, type I mechanism), or a redox product of the sensitizer itself is the active species in the selective treatment of tumors by PDT. The oxidation and reduction potentials of the sensitizer are important variables in studies aimed at uncovering the mechanistic details of this process. The texaphyrin family of complexes provides an excellent opportunity for carrying out such mechanistic investigations.

Acknowledgment. This work was supported by Grant No. 1581 from the Texas Advanced Research Program to J.L.S and by a grant from the Division of Chemical Sciences, Office of Basic Energy Sciences, Department of Energy, under Contract DE-FG05-87ER13789 to T.E.M., J.L.S. and T.E.M. also thank the NSF for Presidental Young Investigator Awards, the Alfred P. Sloan Foundation for Research Fellowships, and the Camille and Henry Dreyfus Foundation for Teacher-Scholar Awards. Grateful acknowledgment is also made to the Midwest Center for Mass Spectrometry for high-resolution mass spectrometric analyses.

Contribution from the Department of Chemistry, Harvard University, Cambridge, Massachusetts 02138

The Cavitand Concept in the Synthesis of Subsite-Differentiated Analogues of Biological [4Fe-4S/Se]$^{2+}$ Clusters: Cluster Capture Reactions, Ligand Conformational Analysis, and the Structure of a Trigonal [4Fe-4Se]$^{2+}$ Analogue

T. D. P. Stack, J. A. Weigel, and R. H. Holm*

Received March 5, 1990

The previously reported clusters $[Fe_4S_4(Me_2LS_3)L']^{2-}$ (L' = RS^-, Cl^-) contain the cubane-type $[Fe_4S_4]^{2+}$ core and are derived from the trithiol $Me_2L(SH)_3$ (**1**, 1,3,5-tris((4,6-dimethyl-3-mercaptophenyl)thio)-2,4,6-tris(*p*-tolylthio)benzene), which as the trianion functions as a semirigid tridentate ligand. Iron sites are differentiated in the ratio 3:1. These clusters are analogous to certain biological clusters that undergo regiospecific reactions at the differentiated Fe site. In this work, the factors that render this unique ligand effective in cluster capture are explored. The reaction $[Fe_4Se_4(SEt)_4]^{2-}$ + **1** yields $[Fe_4Se_4(Me_2LS_3)(SEt)]^{2-}$; treatment of the latter cluster with 1 equiv of *t*-BuCOCl affords $[Fe_4Se_4(Me_2LS_3)Cl]^{2-}$ (**5**). $(Ph_4P)_2$[**5**]·2DMF crystallizes in the trigonal space group *P*3 with a = 24.733 (3) Å, c = 14.595 (3) Å, and Z = 3. The crystal structure consists of the three crystallographically independent clusters with imposed trigonal symmetry; these occur in a Δ:Λ ratio of 2:1 as refined crystallographically. The crystal is inversion-twinned, with only a slight preference for one enantiomer. The $[Fe_4Se_4]^{2+}$ core structures of the three clusters are nearly constant, but ligand conformations, described by tilt and cant angles of the coordinating arms of the ligand, are different. Formation of **5** reveals the flexibility of the ligand, inasmuch as the volume of the $[Fe_4Se_4]^{2+}$ core is 10% larger on the basis of atom coordinates and about 25% larger on the basis of van der Waals radii than that of the $[Fe_4S_4]^{2+}$ core. Cluster structures are analyzed in terms of ligand flexibility and conformation, cavity occupancy, and core structure. The clusters $[Fe_4S_4(Me_2LS_3)Cl)]^{2-}$ and $[Fe_4S_4(t\text{-}BuLS_3)Cl]^{2-}$ were isolated in high yield from the ligand-substitution reactions of **1** and *t*-BuL$(SH)_3$ (**2**, 1,3,5-tris((3-mercapto-5-*tert*-butylphenyl)thio)-2,4,6-tris(*p*-tolylthio)benzene), respectively, with $[Fe_4S_4(SEt)_4]^{2-}$ followed by reaction with pivaloyl chloride. In clear contrast, the related ligand $L(SH)_3$ (**3**), lacking the 4,6-dimethyl or 5-*t*-Bu substituents but otherwise identical, forms a mixture of soluble and polymeric clusters under the same conditions. ^{1}H NMR evidence is presented that the ligands exist in a solution conformation in which the three thiol-containing substituents (arms) are on one side of the central ring and the three *p*-tolylthio groups (legs) are on the other side. Because of the steric directing effects of the ring substituents on the arms of **1** and **2**, these molecules adopt dominant configurations with the three thiol groups turned inward over the central benzene ring. These configurations are recognized by the shielding of protons on the arms near the central ring. They are less populated with **3** because the molecule lacks the orienting effects of ring substituents. This situation is consistent with the results of a molecular dynamics analysis of **1** and **3**. Consequently, **1** and **2** are predisposed to capture a cubane-type cluster in ligand-substitution reactions and to suppress polymer formation. In this regard, these ligands may be considered to possess the principal attribute of cavitand molecules.

Introduction

Recently, we have summarized those structural and reactivity properties of the native cubane-type $Fe_4(\mu_3\text{-}S)_4$ clusters that are specific to a particular Fe subsite,[1-3] which is significantly differentiated by protein structure and environment from the other three subsites. The means of such differentiation are largely unknown and could involve terminal ligands other than cysteinyl thiolate and/or a coordination number exceeding 4. In the case of pig heart aconitase, it has now been established by protein crystallography that one subsite has a hydroxide or water terminal ligand and the other three subsites have conventional cysteinate ligation.[4]

In seeking synthetic analogues of such clusters, we have considered as a reasonable first step the synthesis of a tridentate trithiol ligand capable of spanning three of the subsites of a cluster and, ideally, affording a cluster species of overall trigonal symmetry. In this way, a 3:1 subsite population is created, affording the possibility of specific manipulation of the unique subsite. An approach such as this to analogue clusters is required inasmuch as the usual clusters $[Fe_4S_4(SR)_4]^{2-}$ of effectively cubic core symmetry undergo essentially statistical ligand substitution reactions.[3] Further, those anionic mixed ligand clusters that have been isolated[5] undergo statistical disproportionation in solution, and one cluster, $[Fe_4S_4(SC_6H_4\text{-}2\text{-}OH)_4]^{2-}$ as its Et_4N^+ salt, while crystallizing with one five-coordinate subsite, reverts to four-coordinate, equivalent subsites in solution.[6]

Tridentate ligands in the form of glycyl–cysteinyl oligopeptides have been shown to bind to clusters as products of substitution reactions with $[Fe_4S_4(S\text{-}t\text{-}Bu)_4]^{2-}$ in Me_2SO solution.[7] However,

(1) Stack, T. D. P.; Holm, R. H. *J. Am. Chem. Soc.* **1987**, *109*, 2546.
(2) Stack, T. D. P.; Holm, R. H. *J. Am. Chem. Soc.* **1988**, *110*, 2484.
(3) Holm, R. H.; Ciurli, S.; Weigel, J. A. *Prog. Inorg. Chem.*, in press.
(4) Robbins, A. H.; Stout, C. D. *Proc. Natl. Acad. Sci. U.S.A.* **1989**, *86*, 3639; *Proteins* **1989**, *5*, 289.
(5) (a) Kanatzidis, M. G.; Baenziger, N. C.; Coucouvanis, D.; Simopoulos, A.; Kostikas, A. *J. Am. Chem. Soc.* **1984**, *106*, 4500. (b) Kanatzidis, M. G.; Coucouvanis, D.; Simopoulos, A.; Kostikas, A.; Papaefthymiou, V. *J. Am. Chem. Soc.* **1985**, *107*, 4925.
(6) Johnson, R. E.; Papaefthymiou, G. C.; Frankel, R. B.; Holm, R. H. *J. Am. Chem. Soc.* **1983**, *105*, 7280.
(7) (a) Que, L., Jr.; Anglin, J. R.; Bobrik, M. A.; Davison, A.; Holm, R. H. *J. Am. Chem. Soc.* **1974**, *96*, 6042. (b) Burt, R. J.; Ridge, B.; Rydon, H. N. *J. Chem. Soc., Dalton Trans.* **1980**, 1228.

0020-1669/90/1329-3745$02.50/0